International Journal of Psychophysiology 103 (2016) 149–160

Contents lists available at ScienceDirect

International Journal of Psychophysiology

journal homepage: www.elsevier.com/locate/ijpsycho

The relation between structural and functional connectivity patterns in complex brain networks

C.J. Stam [a,*], E.C.W. van Straaten [a], E. Van Dellen [a,b], P. Tewarie [a], G. Gong [c], A. Hillebrand [a], J. Meier [d], P. Van Mieghem [d]

[a] Department of Clinical Neurophysiology, VU University Medical Center, Amsterdam, The Netherlands
[b] Department of Psychiatry, Brain Center Rudolf Magnus, University Medical Center Utrecht, the Netherlands
[c] National Key Laboratory of Cognitive Neuroscience and Learning, School of Brain and Cognitive Sciences, Beijing Normal University, Beijing, China
[d] Faculty of Electrical Engineering, Mathematics and Computer Science, Delft University of Technology, PO Box 5031, 2600 GA Delft, The Netherlands

ARTICLE INFO

Available online 10 February 2015

Keywords:
Graph theory
Brain dynamics
SIS model
Phase transition
Functional connectivity
Effective connectivity

ABSTRACT

Objective: An important problem in systems neuroscience is the relation between complex structural and functional brain networks. Here we use simulations of a simple dynamic process based upon the susceptible–infected–susceptible (SIS) model of infection dynamics on an empirical structural brain network to investigate the extent to which the functional interactions between any two brain areas depend upon (i) the presence of a direct structural connection; and (ii) the degree product of the two areas in the structural network.
Methods: For the structural brain network, we used a 78×78 matrix representing known anatomical connections between brain regions at the level of the AAL atlas (Gong et al., 2009). On this structural network we simulated brain dynamics using a model derived from the study of epidemic processes on networks. Analogous to the SIS model, each vertex/brain region could be in one of two states (inactive/active) with two parameters β and δ determining the transition probabilities. First, the phase transition between the fully inactive and partially active state was investigated as a function of β and δ. Second, the statistical interdependencies between time series of node states were determined (close to and far away from the critical state) with two measures: (i) functional connectivity based upon the correlation coefficient of integrated activation time series; and (ii) effective connectivity based upon conditional co-activation at different time intervals.
Results: We find a phase transition between an inactive and a partially active state for a critical ratio $\tau = \beta/\delta$ of the transition rates in agreement with the theory of SIS models. Slightly above the critical threshold, node activity increases with degree, also in line with epidemic theory. The functional, but not the effective connectivity matrix closely resembled the underlying structural matrix. Both functional connectivity and, to a lesser extent, effective connectivity were higher for connected as compared to disconnected (i.e.: not directly connected) nodes. Effective connectivity scaled with the degree product. For functional connectivity, a weaker scaling relation was only observed for disconnected node pairs. For random networks with the same degree distribution as the original structural network, similar patterns were seen, but the scaling exponent was significantly decreased especially for effective connectivity.
Conclusions: Even with a very simple dynamical model it can be shown that functional relations between nodes of a realistic anatomical network display clear patterns if the system is studied near the critical transition. The detailed nature of these patterns depends on the properties of the functional or effective connectivity measure that is used. While the strength of functional interactions between any two nodes clearly depends upon the presence or absence of a direct connection, this study has shown that the degree product of the nodes also plays a large role in explaining interaction strength, especially for disconnected nodes and in combination with an effective connectivity measure. The influence of degree product on node interaction strength probably reflects the presence of large numbers of indirect connections.

1. Introduction

There is a growing consensus that the brain can be understood as a complex network both at the structural as well as the functional level (Bassett and Bullmore, 2006; Bullmore and Sporns, 2009; van den Heuvel and Hulshoff Pol, 2010). The network approach has been

* Corresponding author at: Department of Clinical Neurophysiology and MEG Center, VU University Medical Center, De Boelelaan 1118, 1081 HV Amsterdam, The Netherlands. Tel.: +31 20 4440727.
E-mail addresses: CJ.Stam@VUmc.nl (C.J. Stam), P.F.A.VanMieghem@tudelft.nl (P. Van Mieghem).

http://dx.doi.org/10.1016/j.ijpsycho.2015.02.011
0167-8760/

motivated after recognizing that higher brain functions cannot be understood as the sum of local activations and that they require a concept of emergent functions in a network that combines segregation and integration (Sporns, 2013). The study of complex brain networks has been stimulated by the advent of network science, a combination of graph theory, statistical mechanics and dynamical systems theory, and by the progress in structural and functional imaging techniques such as MRI, EEG and MEG (Stam and van Straaten, 2012; van Straaten and Stam, 2013). Brain networks are characterized by a combination of local connectedness as well as global integration; features characteristic of so-called "small-world" networks (Watts and Strogatz, 1998; Sporns, 2013). At a higher level, brain networks consist of sub-networks or modules (resting state networks in the fMRI literature) that sub-serve higher level functions and are interconnected in a hierarchical manner (Kaiser and Hilgetag, 2010; Park and Friston, 2013). Brain networks also have scale-free properties, with a relatively large number of highly connected nodes or "hubs", in particular in the default mode network and association cortex (Barabasi and Albert, 1999; van den Heuvel et al., 2008). Hubs have been shown to be crucially important for normal cognition, but may also constitute vulnerable spots in neurodegenerative disease (van den Heuvel et al., 2009; de Haan et al., 2012). Together a group of strongly interconnected hub areas may form a "rich club" that functions as a core system for information flow in the brain (van den Heuvel et al., 2012; van den Heuvel and Sporns, 2013).

A complex topology of brain networks has been demonstrated in structural as well as functional networks. On a relatively short time scale, where the effects of neuronal growth and learning can be ignored, structural networks can be understood as fixed anatomical connections between distributed brain areas. Functional networks reflect a dynamical process taking place on these fixed structural networks and can be reconstructed by estimating statistical correlations between time series of neural activity of the brain areas (Pereda et al., 2005). Functional connectivity refers to the existence of statistical correlations, while effective connectivity aims to identify directed causal influence of one brain area on another (Gerstein and Aertsen, 1985; Friston et al., 2013). How structural brain networks determine functional brain networks is an open question in brain network research (Rubinov et al., 2009; Honey et al., 2010; Ponten et al., 2010). A better understanding of this relationship could help to predict how changes in brain network structure can give rise to abnormal dynamics and disease (Honey and Sporns, 2008; Kaiser, 2013; van Dellen et al., 2013).

Evidence from empirical studies suggests that the presence of a direct anatomical connection between two brain areas is associated with stronger functional interactions between these two areas (Honey et al., 2007, 2009; Rubinov et al., 2009; Hermundstad et al., 2013). However, functional interactions have also been detected between brain areas without direct anatomical connections (Honey et al., 2007, 2009). Several studies have attempted to address this problem by simulating brain dynamics on structural networks based upon anatomical data from animals or humans (Honey et al., 2007, 2009; Rubinov et al., 2009; Ponten et al., 2010; Deco et al., 2011, 2012, 2013). Using a structural network of the macaque and a nonlinear model of brain dynamics, Honey et al. (2007) showed that functional networks strongly resemble structural networks at long time scales (minutes), but not at short time scales (seconds). These results were confirmed in a study using human structural brain network data (Honey et al., 2009), where it was shown that part of the functional connectivity could be due to indirect (length two) connections between brain areas. Another important result is the observation that functional networks resemble structural networks more strongly if the dynamical system is close to a phase transition (Rubinov et al., 2011; Haimovici et al., 2013). This is of interest since critical brain dynamics may be an optimal state for information processing (Shew and Plenz, 2013). Finally, there is growing evidence that the details of the dynamical system may be relatively unimportant for understanding the structure function relations if the system is near a critical point (Deco et al., 2012; Haimovici et al., 2013). This suggests that very simple dynamical systems could be used to investigate the functional and effective connectivity between brain areas as a function of their topological relation.

In the present study, a simple dynamical model, derived from the theory of epidemics, is applied to simulate brain dynamics on a structural network of 78 interconnected brain regions based upon DTI data of 80 healthy subjects (Gong et al., 2009). The dynamical model was analogous to the SIS (susceptible–infected–susceptible) model of infection dynamics, where each node (brain area) can be in two states (excitable and activated) with the transitions determined by two transition probabilities β and δ. The SIS model on networks is well-studied and we can benefit from its mathematical knowledge concerning this type of dynamics, for instance with respect to the epidemic threshold (Van Mieghem et al., 2009; Castellano and Pastor-Satorras, 2010; Boguñá et al., 2013; O'Dea et al., 2013; Wang et al., 2013). We addressed the following questions: (i) What is the relation between structural and functional networks close to and further away from the epidemic threshold and do the results for the SIS model on networks resemble those for more sophisticated models such as various types of neural mass models? (ii) Which aspects of structure function relations are detected by different connectivity measures? For this purpose we compare simplified functional and effective connectivity measures. (iii) Does structural degree of brain areas influence the strength of functional interactions in the absence of a direct connection?

2. Methods

2.1. Structural connection matrix

We used a binary symmetric structural matrix (where connections are either absent or present) based upon the work of Gong et al. (Gong et al., 2009). In this study in 80 healthy subjects, connections (edges) between 78 cortical regions (the vertices or nodes), defined according the automatic anatomical labeling atlas (Tzourio-Mazoyer et al., 2002), were determined with probabilistic tractography. The binary group level matrix consisted only of edges that were significant in the whole group of 80 subjects. The resulting binary matrix is shown in Fig. 1B. The same matrix was used in previous studies (de Haan et al., 2012; van Dellen et al., 2013; Tewarie et al., 2014).

2.2. Model dynamics

To model the dynamics of the brain areas, we used a simple scheme derived from epidemics on complex networks. In the infection model each node can be in one of three states: "susceptible", "infected" and "recovered". Transitions between these states are described by rates (in continuous-time Markov chains) or transition probabilities (in discrete-time Markov chains). In the present study, we restrict ourselves to a discrete-time analysis of the SIS model in which we replace "susceptible" with "excitable" and "infected" with "activated". We define two the transition probabilities as β (probability of transition between state E [excitable] and state A [activated]) and δ (probability of transition between state A and E). Two nodes can only interact if they are connected by an edge. Time is discrete, and updating all node states is synchronous. If a node is activated at time n, it can activate at time $n + 1$ any direct neighbor with a probability β. Its own state will change to excitable at time $n + 1$ with a probability δ. If a node is excitable at time n, it will be activated at time $n + 1$ if it is activated by at least one of the active nodes to which it is connected. At the beginning of each run (time $n = 1$) of 4096 time steps all nodes are excitable with the exception of 20% of the nodes chosen at random which are activated. The overall dynamics of the model is determined by the effective infection probability $\tau = \beta/\delta$. We choose to fix δ at 0.5, which means that each node activated at time n will be excitable at time $n + 1$ with a probability of 0.5. We define the overall activation of the system as the average fraction of activated nodes. The critical value β is defined as

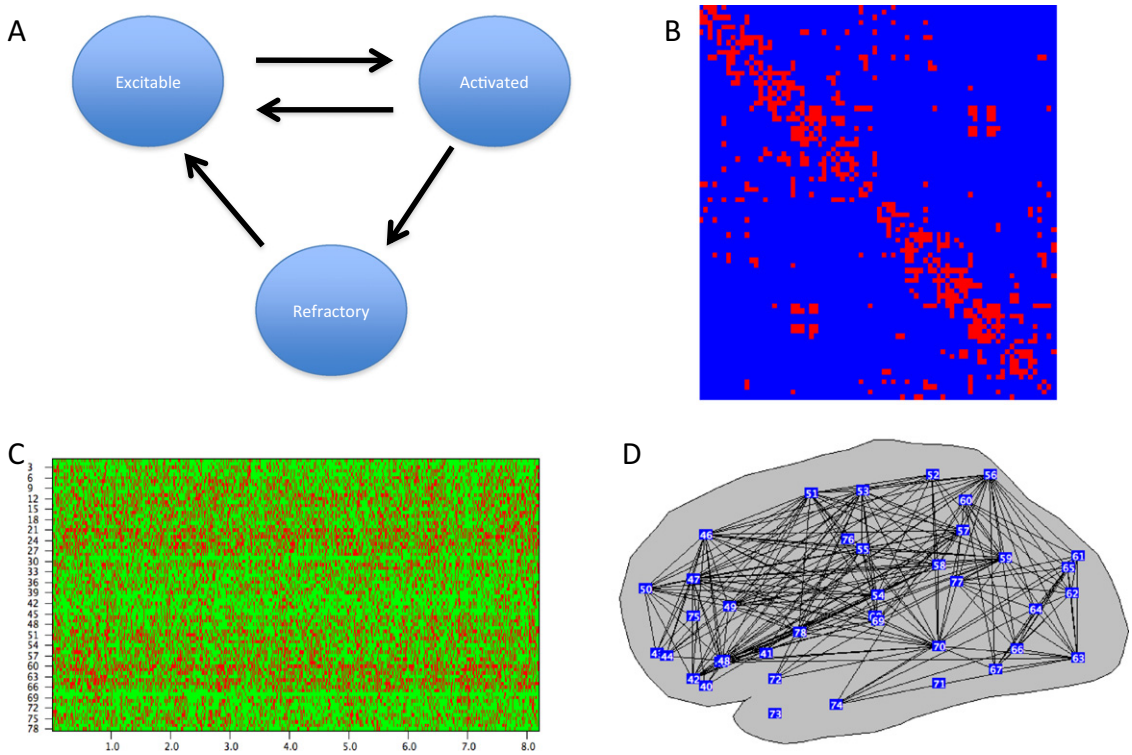

Fig. 1. Schema of the model. (A) General schema of the dynamics of the model. Each node can be in one of three states: excitable, activated or refractory (these states are similar to the susceptible, infected and recovered states in the SIRS model). Transitions between different states are determined by probabilities indicated by arrows. In the present study we restrict ourselves to the excitable and activated state and the two corresponding probabilities (equivalent to a SIS model). (B) Binary matrix of structural connections between 78 nodes. Each node corresponds to a brain area of the AAL atlas (Tzourio-Mazoyer et al., 2002). Red indicates a connection between two areas, blue no connection. The structural matrix is based upon Gong et al. (2009). (C) Example of the dynamics of the system. The horizontal axis corresponds to time (4096 discrete time points). The vertical axis corresponds to the 78 AAL regions. Green indicates the excitable state of a node, red the activated state. (D) A functional network can be reconstructed by computing the correlations between time series of node activation, for all possible pairs of nodes. In (D) all correlations exceeding a certain threshold are indicated by a line between the corresponding brain regions.

the value of β for which the overall activation is on average 1% of the average maximal activation of 1 for any value of β.

2.3. Functional and structural connectivity

Time series of node activation states were used to determine the strength of functional interactions between each node pair. Two approaches were used, each based upon a different way to characterize the functional interaction between nodes. In the first case, referred to as "functional connectivity", we computed the Pearson correlation coefficient of integrated node activation time series of pairs of nodes. Node states were coded as excitable = 0, and activated = 1. The original time series of consecutive one's and zero's was replaced by an integrated time series (defined below) where the value of X_n at time n was equal to the sum of values R_n in the original time series over an integration interval w:

$$X_n = \frac{1}{w}\sum_{i=1}^{w} R_{n+i}. \quad (1)$$

In the present study we used an integration window w = 10, but results were quite similar for a range of values w between 1 and 50. The Pearson correlation coefficient was computed from the time series X and Y as follows:

$$C_{func} = \frac{\sum (X - \langle X \rangle)(Y - \langle Y \rangle)}{\sqrt{(X - \langle X \rangle)^2 (Y - \langle Y \rangle)^2}}. \quad (2)$$

Here $\langle\rangle$ is the average value.

The second measure, referred to as "effective connectivity" was designed to capture more directly the causal flow between pairs of nodes. The effective connectivity from node X to node Y was defined as the probability that $Y_{n+d} = 1$ if $X_n = 1$. The effective connectivity from Y to X was defined as the probability that $X_{n+d} = 1$ if $Y_n = 1$. Since we used an undirected structural network to simulate the dynamics we decided to use the sum of effective connectivity from X to Y and Y to X as our final, now symmetrical, effective connectivity measure:

$$C_{eff} = p(Y_{n+d} = 1 | X_n = 1) + p(X_{n+d} = 1 | Y_n = 1). \quad (3)$$

Here, C_{eff} is the effective connectivity between X and Y depending on the chosen time lag d, Pr[.] denotes the probability operator (on random variables or events), n is discrete time and d is the length of an interval. In the simulations we used d = 1.

2.4. Graph theoretical analysis

For each simulation run, we computed the average functional and effective connectivity for all pairs of nodes, resulting in a symmetric 78 × 78 matrix of connectivity values between 0 and 1 (although C_{eff} can take on values >1, in our simulations values were always between 0 and 1). The length of the time series used for computation of the connectivity was taken from n = 1 to n = final, such that none of the nodes was active for any time after n = final, where final ≤ 4096. This was important since close to criticality the length (in number of discrete time steps) of the activations fluctuated strongly, and thus final could be shorter than 4096. Next, connectivity matrices for 100 different runs were averaged to obtain one average matrix of functional or effective connectivity.

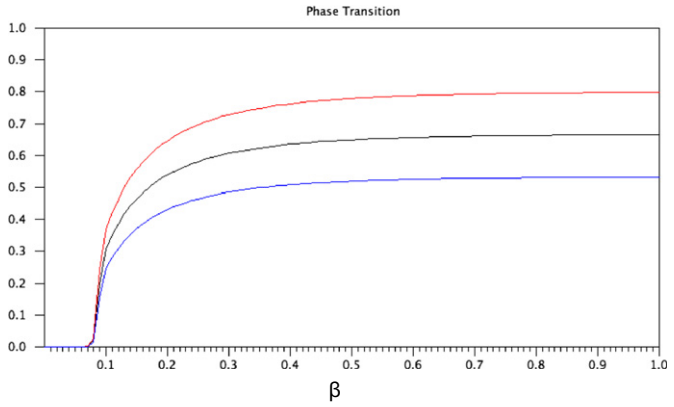

Fig. 2. Phase transition in the SIS model. The fraction of activated nodes is shown as a function of increasing values of the probability β, from 0 to 1 in steps of 0.01, for a constant value of $\delta = 0.5$. The black line is the average value for 10 runs, each consisting of 4096 time steps. Red and blue lines indicated the standard deviation. A phase transition can be seen close to rate $\beta = 0.08$.

These averaged connectivity matrices were analyzed in two ways. First, the complete weighted matrices were converted into unweighted binary matrices with the exact same number of edges as the structural matrix. For the structural matrix and the binarized average functional and effective connectivity matrix the modular structure was determined using Newman's statistic Q_m for modularity (Newman and Girvan, 2004) and a simulated annealing approach as described in Stam et al. (2010). The modularity of the connection matrix was determined using the approach of Guimerà and Nunes Amaral (2005). The modularity index Q_m is defined as:

$$Q_m = \sum_{s=1}^{m}\left[\frac{l_s}{L} - \left(\frac{d_s}{2L}\right)^2\right]. \quad (3)$$

Here, m is the number of modules, l_s is the number of links in module s, L is the total sum of all links in the network, and d_s is the sum of the degrees of all vertices in module s. A simulated annealing algorithm was used to find the optimal way to divide the network into modules. Initially, each of the N nodes was randomly assigned to one of the m possible modules, where m was taken as the square root of N. At each step, one of the nodes was chosen at random, and assigned a different random module number from the interval {1,..,N}. Modularity Q_m was calculated before and after this node re-assignment. The cost C for the simulated annealing algorithm was defined as $-Q_m$. The new partitioning was preserved with probability p

$$p = \begin{cases} 1 \text{ if } C_f \le C_i \\ e^{-\frac{C_f - C_i}{T}} \text{ if } C_f > C_i \end{cases} \quad (4)$$

where C_f is the final cost and C_i is the initial cost. The temperature T was 1 initially, and was lowered once every 100 steps as follows: $T_{new} = 0.995 \cdot T_{old}$. In total, the simulated annealing algorithm was run for 10^6 steps.

Second, the data of the original complete weighted matrices were analyzed. For the average connectivity matrix, obtained by averaging over 100 runs, we determined the average strength of the functional

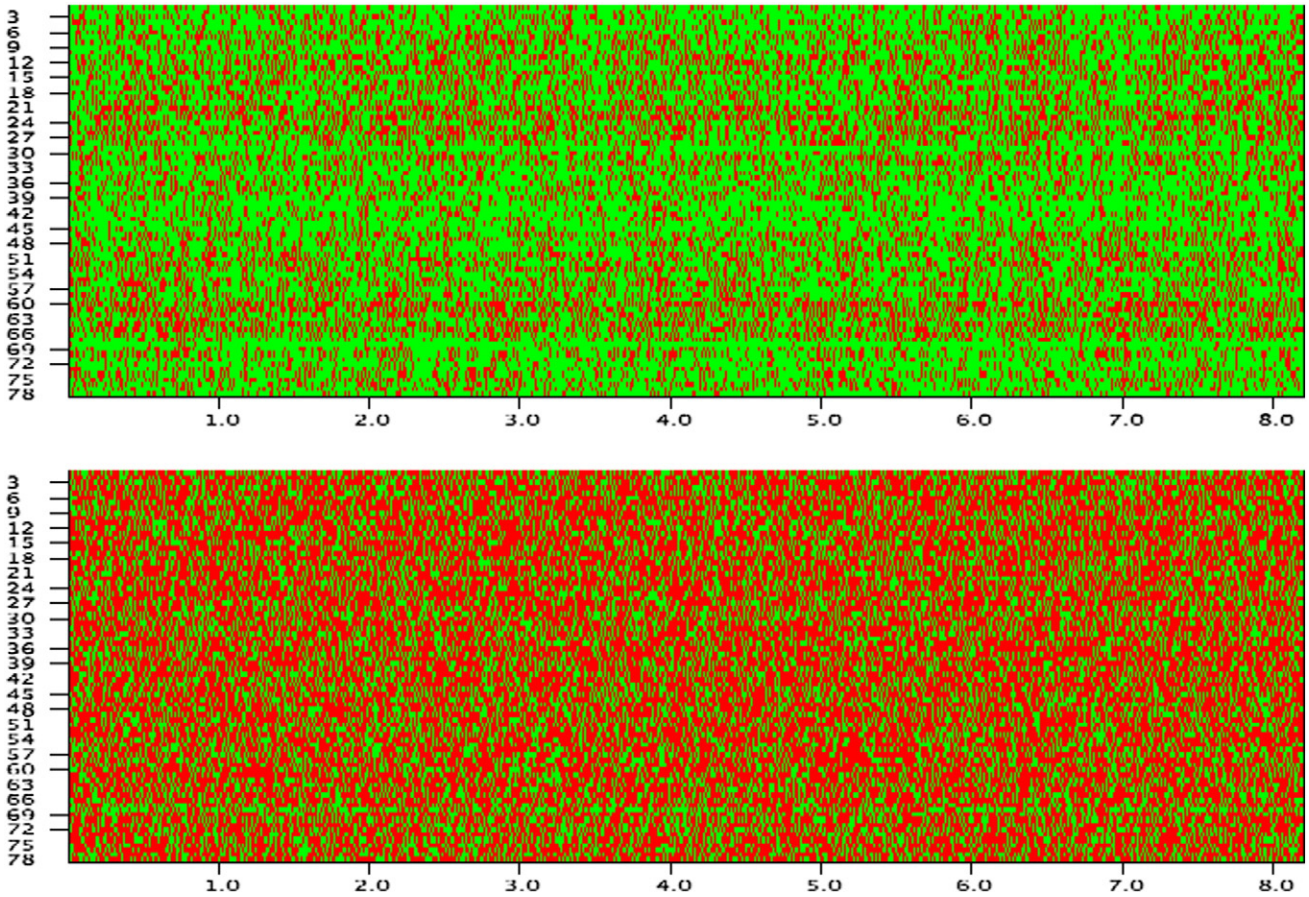

Fig. 3. Spatial temporal dynamics close to and away from transition. Illustration of the model dynamics close to and further away from the critical ratio of β/δ. The horizontal axis corresponds to discrete time from 1 to 4096. The vertical axis corresponds to the 78 brain regions. Green indicates the excitable state, red the activated state. In panel A the dynamics is shown for rate $\beta = 0.1$ and rate $\delta = 0.5$. In panel B the dynamics is shown for $\beta = 0.5$ and $\delta = 0.5$. The overall activity increases with a higher value of β. Only for the lower value of $\beta = 0.1$ is it possible to discern nodes with relatively high and relatively low activity.

or effective connectivity of the whole matrix W(mean), as well as subaverages for all node pairs with [W(connect)] or without [W(disc)] an edge in the structural matrix, disregarding self-loops. Next, the functional and effective connectivity values for each node pair of the whole matrix were plotted against the product of the corresponding degrees in the structural matrix. A linear regression was fitted to the data, and the intercept and slope were determined (Barrat et al., 2004). The same procedure was applied to degree preserving random networks (Maslov and Sneppen, 2004). Statistical comparison of functional and effective connectivity obtained for the original and random structural networks was done by repeating the whole procedure 20 times and using a t-test for independent samples, assuming unequal variance, to determine significant differences between results for original and random networks.

3. Results

3.1. Unweighted network analysis

Since our goal was to study the nature of the dynamic process, and in particular the statistical relations between time series of node activation, close to a phase transition, we first determined the critical point of the dynamics where a sudden increase in average activity is observed for a small change of the ratio $\tau = \beta/\delta$. In the SIS epidemics on networks, it is known that this transition (the "epidemic threshold τ_c") is determined by the ratio of the transition probabilities between the "susceptible" and "infected" states. In our model this translates to the ratio $\tau = \beta/\delta$. The SIS theory (see e.g. Van Mieghem and van de Bovenkamp, 2013) shows that $\tau_c > 1/\lambda_1$, where λ_1 is the largest eigenvalue of the adjacency matrix (for the present Gong network: $\lambda_1 = 10.470$). To confirm this theoretical result, we first determined the critical ratio by simulations. The SIS model was simulated for values of β between 0 and 1, increasing in steps of 0.01, and a fixed probability of $\delta = 0.5$. The average and standard deviation of the mean activation were obtained for 10 runs for different values of β. The results are shown in Fig. 2. A clear transition can be seen between a state with no activity and a state with increasing average activity levels near $\beta = 0.07$. For the rest of this study we used a slightly higher value of probability $\beta = 0.08$, where the average activity was 1% of the maximal activity for any value of β. For comparison we also studied a state further away from the critical point with $\beta = 0.2$.

An example of the dynamical patterns that can be observed in the model is shown in Fig. 3. The figure shows the activation state of the nodes (green = excitable, red = activated) as a function of time (4096 time steps). For $\beta = 0.1$ and $\delta = 0.5$ a clear pattern can be seen, with nodes alternating between the two states, and some nodes

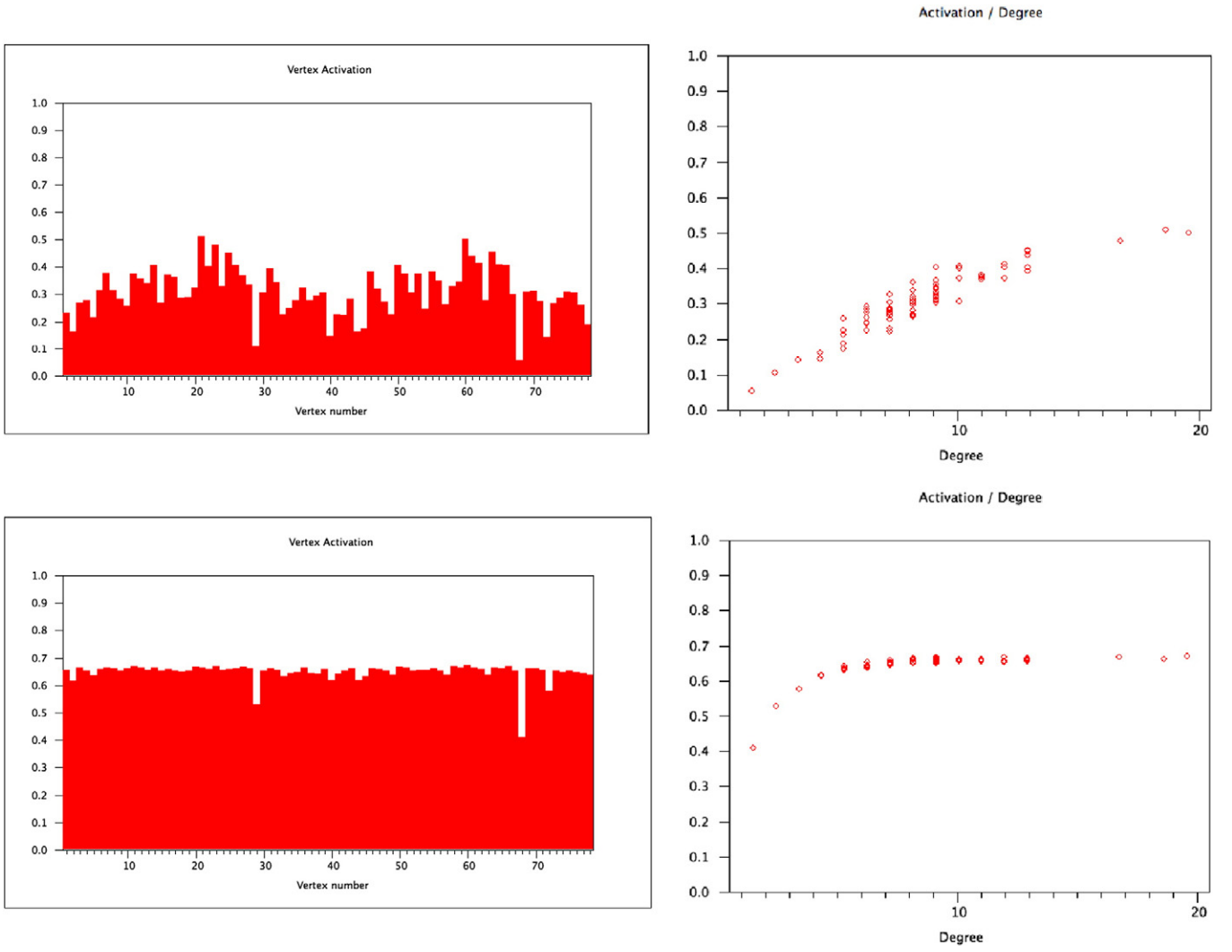

Fig. 4. Activity of individual ROIs and as function of degree. (A) Activity of each of the 78 brain areas averaged over a run of 4096 time steps for $\beta = 0.1$ and $\delta = 0.5$. Differences in mean activity can be clearly seen. (B) Mean node activity for the same settings plotted as a function of the node degree. Node activity increases with node degree. (C) The same as in A, but now for $\beta = 0.5$. Almost all nodes show the same high level of activity, with a few exceptions (nodes 29 left Heschl gyrus and 68 right Heschl gyrus). (D) Same plot as C, now for $\beta = 0.5$. Mean activity increases rapidly as function of degree, and subsequently flattens out.

displaying higher levels of activity than others. In the lower panel the activity time pattern is shown for $\beta = 0.5$ and $\delta = 0.5$. Clearly, there is a general increase in the level of activity. At the same time, the differences in activity levels between the 78 brain regions become less distinct.

To explore the differences in activation between the 78 nodes in more detail, average activation of all nodes is shown in Fig. 4. For a relatively low level of activation ($\beta = 0.1$; $\delta = 0.5$) clear differences in node activation can be seen (panel A). Panel B illustrates that these differences can be explained to a large extent by the structural degree of the nodes (see e.g. Van Mieghem, 2012). Average node activation increases as a function of node degree, and only levels off for high degrees. Panel C shows that for a high activation state far from the critical point ($\beta = 0.5$, $\delta = 0.5$) average activation is at the same high level for all nodes, with the exception of AAL region 29 (left Heschl gyrus) and AAL region 68 (right Heschl gyrus). Of interest, these regions are the most poorly connected of the whole structural network. Panel D shows that activation as a function of structural node degree increases very steeply, and then levels off. This preliminary analysis confirms, in line with epidemic theory (see e.g. Van Mieghem, 2012), that the most interesting patterns are more likely to be observed close to the critical point. In fact, the probability that a node j is activated is proportional to the j-th component of the principal eigenvector of the adjacency matrix belonging to eigenvalue λ_1. In addition, the principal eigenvector is, for some networks, close to the degree vector (Van Mieghem, 2013).

In the next step, we compare average matrices of functional and effective connectivity with the underlying structural matrix. Matrices were averaged over 100 separate runs of the model using $\beta = 0.08$

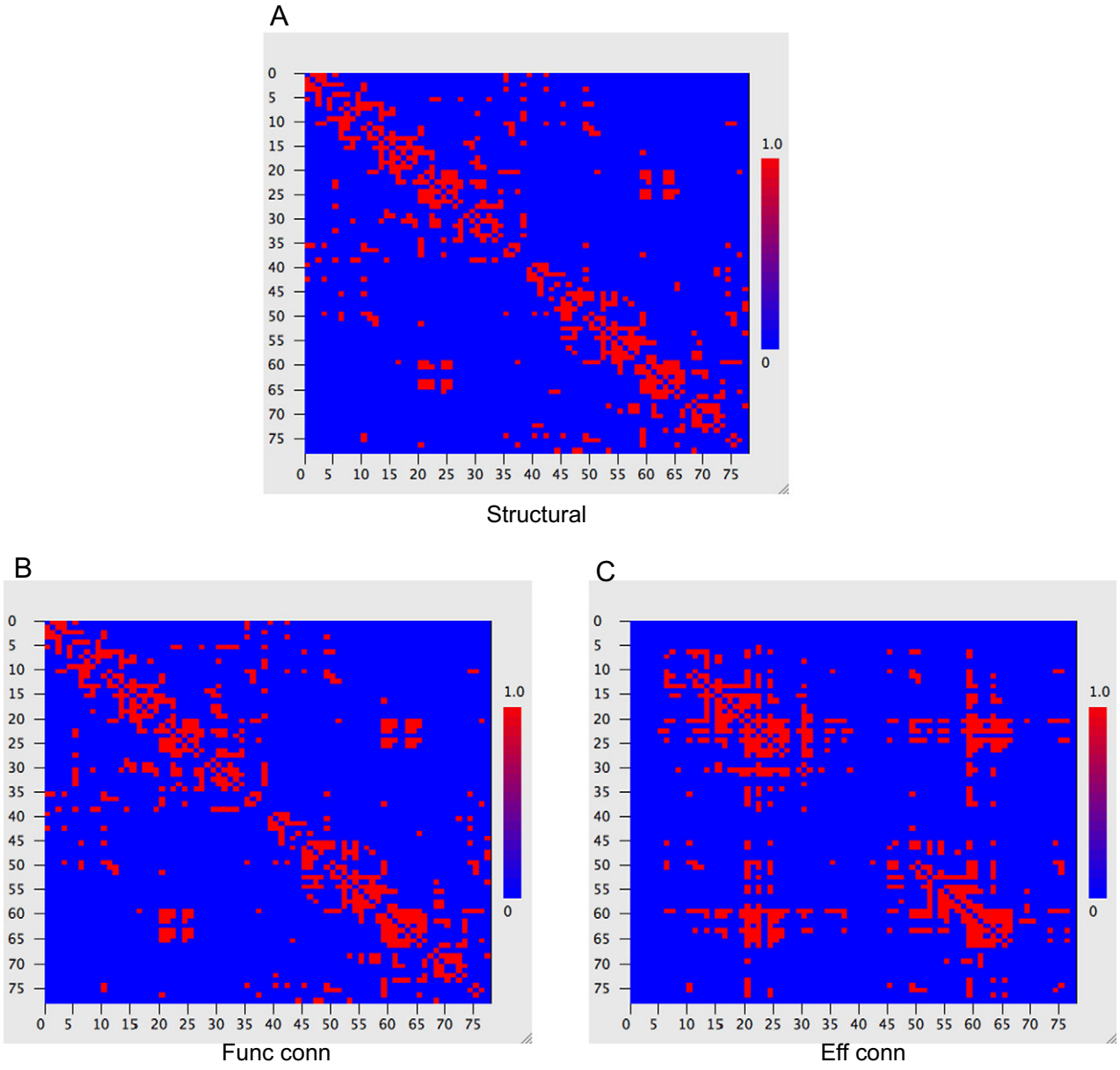

Fig. 5. Binary matrices for structural network, functional and effective connectivity. (A) Structural connectivity matrix for all 78 brain regions. Connections are indicated in red, absence of a connection is indicated in blue. (B) Binary matrix based upon average functional connectivity matrix obtained from 100 runs of each 4096 time steps. The weighted matrix was thresholded such that the number of supra-threshold connections was the same as in the structural matrix in A. Note the almost perfect resemblance between the thresholded functional connectivity and the structural connectivity matrix. (C) Thresholded effective connectivity matrix based upon 100 runs of 4096 time steps with the same number of supra-threshold connection as in A. Note that this matrix shows a clearly different pattern than the ones in A and B.

and $\delta = 0.5$. The complete weighted matrices were then converted to binary matrices with the same number of edges as the original structural matrix. In Fig. 5 the original structural matrix is shown in panel A, the binarized averaged functional connectivity matrix in panel B and the binarized averaged effective connectivity matrix in panel D. On visual inspection there is a striking resemblance between the structural matrix and the binarized version of the functional connectivity matrix. In contrast, the binarized version of the effective connectivity matrix looks quite different compared to both the structural as well as the functional connectivity matrix. In the case of the effective connectivity matrix the pattern is dominated by four large "blobs", two on the diagonal, and two off the diagonal. Many of the edges close to the diagonal, present in panel A and B, are now missing.

One important characteristic of resting-state networks is the presence of a number of sub-networks, referred to as resting state networks (RSN) in the fMRI literature. We determined the modular structure of the original structural matrix and the two functional networks using Newman's modularity statistic Q and a simulated annealing algorithm (Guimerà and Nunes Amaral, 2005; Stam et al., 2010). The results are shown in Fig. 6. In the case of the structural network a number of modules can be distinguished. In the midline a frontal and a posterior module can be seen, that together resemble the default mode network. In both hemispheres a superior frontal parietal network can be seen, as well as a more basal temporal network. The modular organization of the functional connectivity network is quite similar to the structural network. The small differences can be explained by the stochastic nature of the simulated annealing procedure. The effective connectivity network also displays two well-developed midline modules and two slightly less pronounced lateral frontal parietal modules. In contrast to the structural and the functional connectivity network the basal temporal modules are not very clear.

3.2. Weighted network analysis

So far we considered binary versions of the average functional and effective connectivity matrices, and compared these with the binary structural matrix. This approach discards a lot of the information available in the connectivity matrices since these are complete weighted graphs. As a next step we analyzed these fully weighted matrices, and related the weight of all possible pairs of nodes to the product of their respective structural degrees.

The results for functional connectivity are shown in Fig. 7. The fully weighted functional connectivity matrix for $\beta = 0.08$ and $\delta = 0.5$ averaged over 100 runs is shown in Fig. 7A. As expected, this matrix shows a resemblance with the underlying structural matrix as shown in Fig. 5A. However the functional connectivity matrix in Fig. 7A shows additional information, since there is a considerable variation in weights that cannot be simply explained by the presence or absence of a direct link. In Fig. 7B the weights are plotted as a function of their structural degree product on a double logarithmic scale. This plot shows that weights of directly connected nodes (red) are clearly higher than those of nodes without a direct connection (blue). However, the weights for all connections, irrespective of being a directly or indirectly connection, are influenced by the degree products, shown by the slope of the regression line based upon all weights. Functional connectivity between nodes without a direct connection increases as a function of the structural degree product. Further away from the critical point, with $\beta = 0.2$ and $\delta = 0.5$, a different pattern is seen. The average functional connectivity matrix shown in Fig. 7C still resembles the underlying structural matrix, but average connectivity values are lower. The plot of weights as a function of the degree product in Fig. 7D again shows higher weights for directly connected nodes. However, the slope of the regression line based upon all weights is now close to zero. Surprisingly, for the weights of

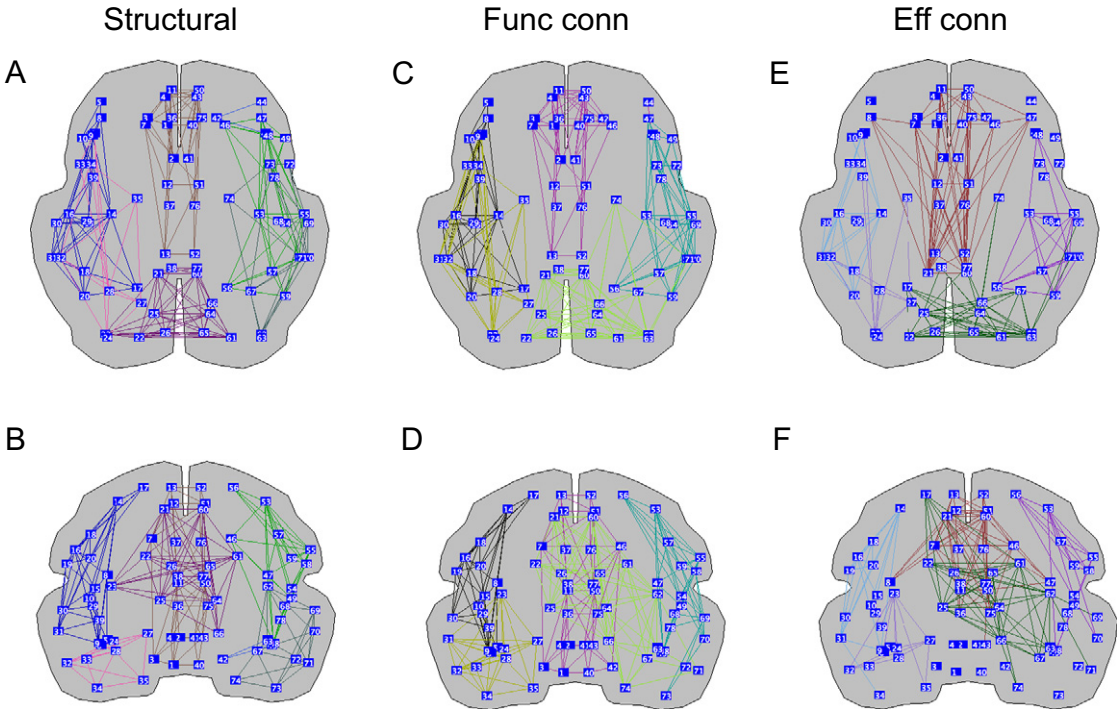

Fig. 6. Modularity for structural network, functional and effective connectivity. Modularity analysis of structural, functional and effective connectivity matrices as shown in Fig. 6. Modularity was determined with a simulated annealing algorithm using Newman's modularity measure. Only within module connections are shown, with a different color for each module. (A) Modules of the structural connectivity matrix. Six modules were found, two in the left hemisphere (basal temporal, and superior frontoparietal); two similar modules in the right hemisphere, one medial frontal module, and one medial parietooccipital module. The last two modules correspond to a large extent with the anterior and posterior parts of the default mode network. (B) Coronal view of the same modules. (C) and (D): modules derived from the functional connectivity matrix. Note the strong resemblance to A and B. (E) and (F): modules based upon the effective connectivity matrix. The pattern is more or less similar as the one of the structural and functional connectivity matrices, but the lateral hemispherical modules stand out less clearly.

connected nodes only, a negative relation between weight and degree product can be seen.

Results for the effective connectivity are illustrated in Fig. 8. In Fig. 8A, for $\beta = 0.08$ and $\delta = 0.5$ a very regular "striping" pattern can be seen, that is rather different from the underlying structural matrix (Fig. 5A). Again connectivity weights are higher for directly connected nodes (red) compared to indirectly connected nodes (blue) (Fig. 8B). Now both types of weights show a scaling with the degree product. The slope of the linear regression line is 0.4671. Thus the strength of the effective connectivity between both directly connected and indirectly connected nodes increases with the degree product. Further away from the critical point for $\beta = 0.2$ and $\delta = 0.5$ the pattern becomes more smooth and the average weight decreases (Fig. 8C). The difference between the average weight of connected compared to indirectly connected nodes becomes smaller, and the slope of the regression line decreases (Fig. 8D).

To investigate the influence of the specific topology of the original structural matrix the experiments were repeated for random networks with the same degree distribution of the original structural matrix (Fig. 9). Only the critical state with $\beta = 0.08$ and $\delta = 0.5$ was studied. The functional connectivity matrix, averaged over 100 runs on a random network, showed a blurred pattern (Fig. 9A). Although the structure of Fig. 7A was lost, a tendency for higher weights closer to the diagonal can still be seen as a result of the preserved degree distribution. Weights for nodes with a direct link were higher than for those with only indirect links, and weight increased as a function of the degree product (Fig. 9B). For effective connectivity (Fig. 9C) the average matrix showed a striping pattern with few other distinctive features. As shown in Fig. 9C weights of directly connected nodes were higher than those of indirectly connected nodes, and all weights increased with degree product, although the slope of the regression line was smaller (0.35) compared to panel B.

To determine the statistical differences between the dynamics simulated on the original structural and the random networks, the experiments were all repeated 20 times for the critical state with $\beta = 0.08$ and $\delta = 0.5$. The results are shown in Table 1. For functional connectivity, the scaling of the weight as a function of the degree product was not statistically different for the original network compared to random networks. Average mean weight and weight for directly connected nodes were significantly higher for original compared to random networks. For effective connectivity, the slope of weight as function of degree

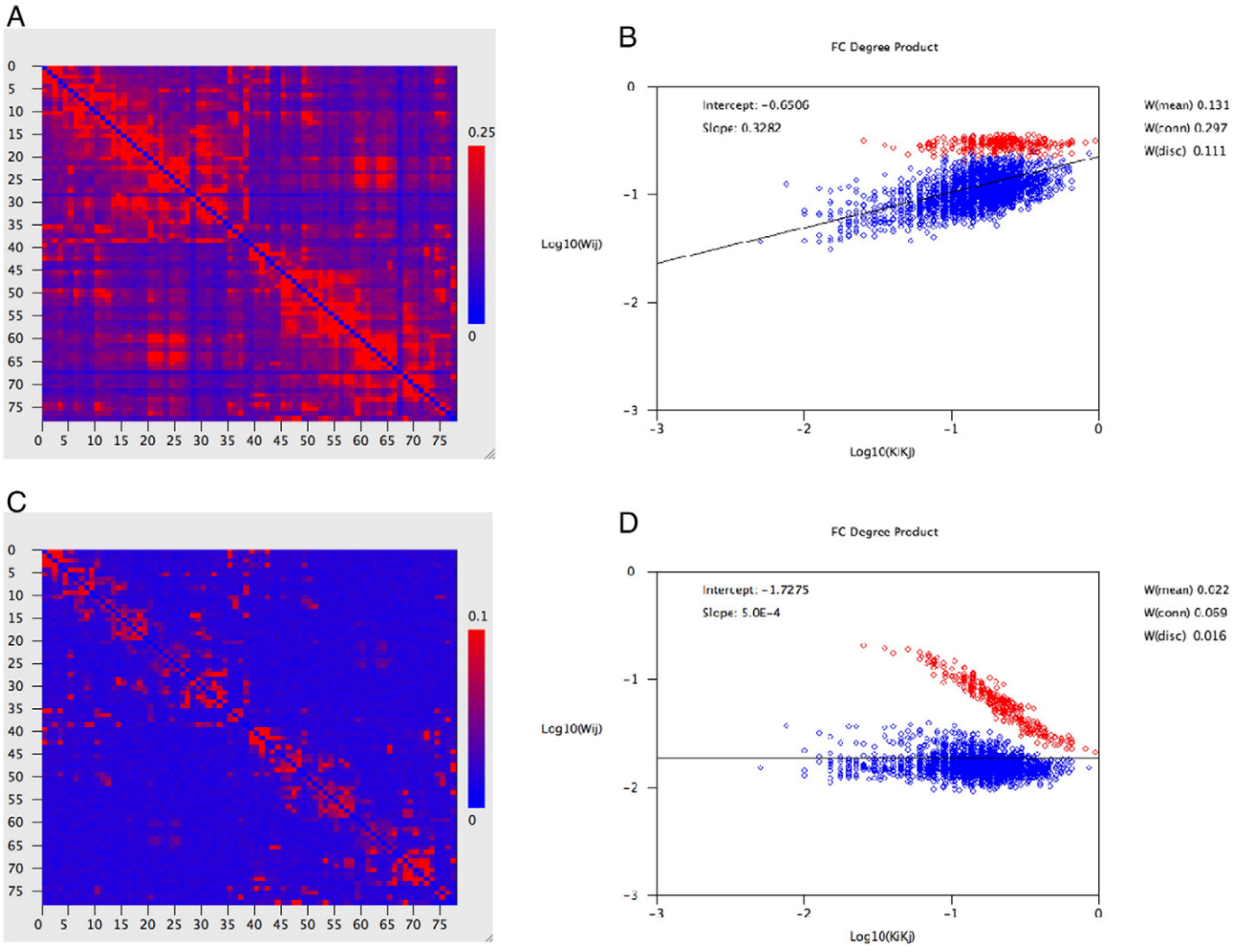

Fig. 7. Functional connectivity plot and FC vs degree product. (A) Matrix of functional connectivity, averaged over 100 runs of each 4096 time steps. Numbers correspond to AAL brain regions. Probability $\beta = 0.08$ and $\delta = 0.5$. Note the resemblance of the functional connectivity matrix to the structural matrix as shown in Fig. 2B. (B) Double logarithmic plot of average functional connectivity of all pairs of areas as a function of the product of their node degrees, using the same settings as in A. Red dots correspond to node pairs with a direct structural connection, blue dots to node pairs without a direct connection. The line is a linear regression based upon all the data (intercept and slope shown in upper left corner). The value W(mean) is the average functional connectivity of all node pairs; W(conn) the average of all connected node pairs, and W(disc) the average of all disconnected pairs. Note the separation of red and blue points. (C) Matrix of average functional connectivity as in A, now for $\beta = 0.2$. (D) Double logarithmic plot of average functional connectivity of all pairs of areas as a function of the product of their node degrees, using the same settings as in C. Red dots are clearly above the blue dots, and show a remarkable negative relation with degree product.

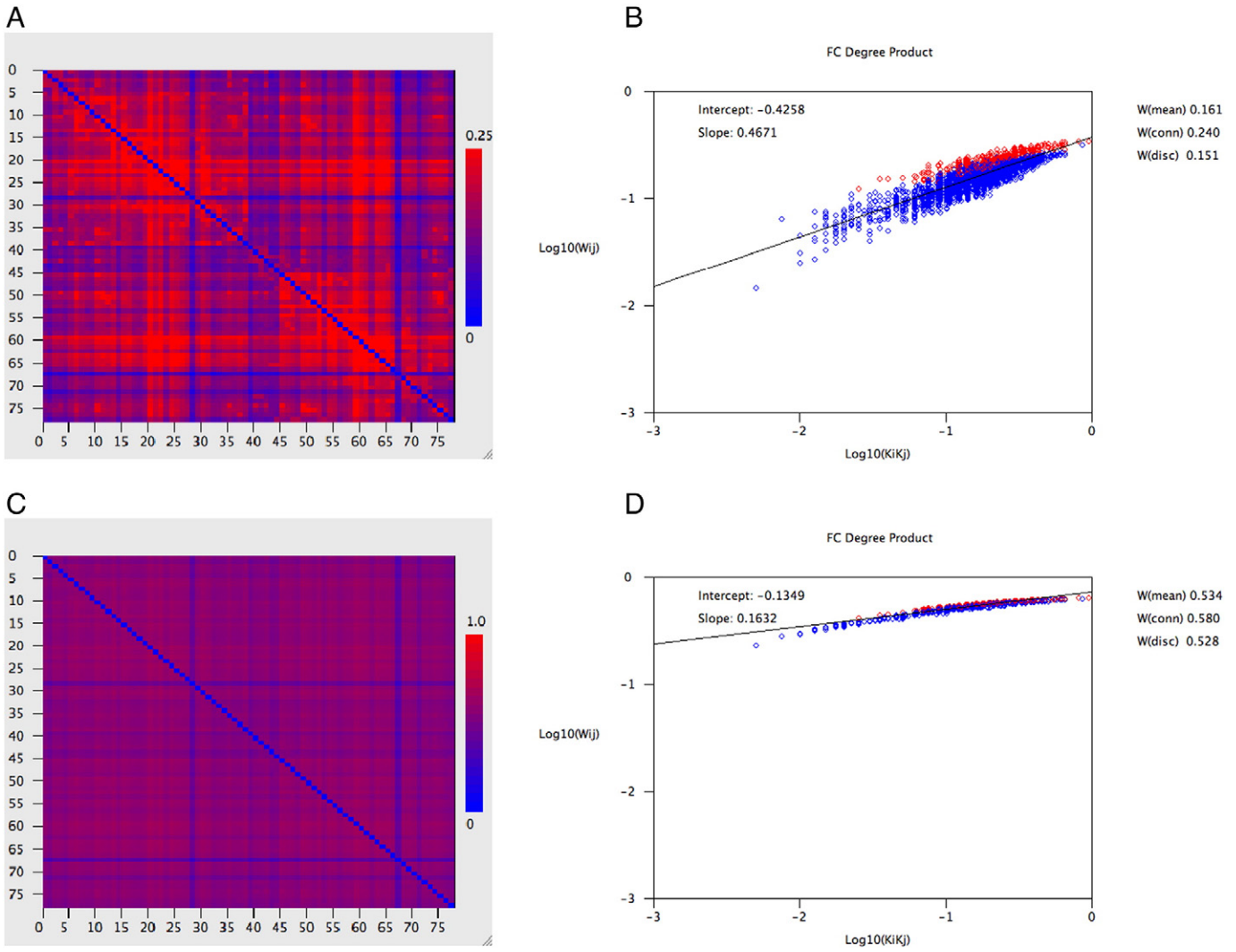

Fig. 8. Effective connectivity plot and EC/degree product. (A) Matrix of effective connectivity, averaged over 100 runs of each 4096 time steps. Numbers correspond to AAL brain regions. Probability $\beta = 0.08$ and $\delta = 0.5$. Note the different pattern of the effective connectivity matrix compared to the functional connectivity matrix as shown in Fig. 7A. (B) Double logarithmic plot of the average effective connectivity of all pairs of areas as a function of the product of their node degrees, using the same settings as in A. Red dots correspond to node pairs with a direct structural connection, blue dots to node pairs without a direct connection. The line is a linear regression based upon all the data (intercept and slope shown in left upper corner). W(mean) is the average functional connectivity of all node pairs; W(conn) the average of all connected node pairs, and W(disc) the average of all disconnected pairs. Note the scaling of connection weights as a function of degree product. (C) Matrix of average effective connectivity as in A, now for $\beta = 0.2$. (D) Double logarithmic plot of effective functional connectivity of all pairs of areas as a function of the product of their node degrees, using the same settings as in C. A similar type of scaling as shown in B but with a smaller slope can be seen.

product was higher for the original network (0.448) compared to the random networks (0.378). Average weight for all nodes and for the indirectly connected nodes were significantly lower for the original networks.

4. Discussion

This study showed that patterns of functional interactions between brain regions can be studied with a simple model derived from the SIS epidemics on networks. Close to a critical point functional interactions were stronger between directly connected areas. A simple functional connectivity measure produced functional networks that were almost identical to the underlying structural network, with the same modular structure. Functional networks derived from effective connectivity did not resemble the structural network, but showed a striking relation between connectivity weight and structural degree product, for connected as well as disconnected points. Together these findings suggest that close to a critical point (i) functional interactions are stronger between directly connected nodes; (ii) connectivity weights of disconnected nodes are not random but depend upon the structural degree product; (iii) the nature of the connectivity measure (functional or effective) has a strong influence upon the observed functional network.

The first question we addressed in this study concerned the relation between structural and functional networks close to and further away from the critical state. One advantage of the use of the SIS epidemic model on networks is that we can build upon the extensive understanding of this model, including the existence of a critical transition ("epidemic threshold"). Theoretically this transition is determined by the ratio of two transition rates, in our case $\tau = \beta/\delta$. Simulations of our model agree with SIS theory: as described in the results section, the phase transition at τ_c occurs at a slightly higher value than $1/\lambda_1$. Manipulation of the ratio of the two rates allowed us to explore the dynamics of the system close to and further away from the critical state. The most interesting results were obtained close to the critical state where the functional connectivity network closely resembled the structural brain network and the effective connectivity network showed a remarkable dependence of the connectivity weight upon the degree product.

There is increasing evidence from empirical studies that resting-state functional brain networks may reflect a state close to a phase transition (Haimovici et al., 2013; Yu et al., 2013). Computational studies

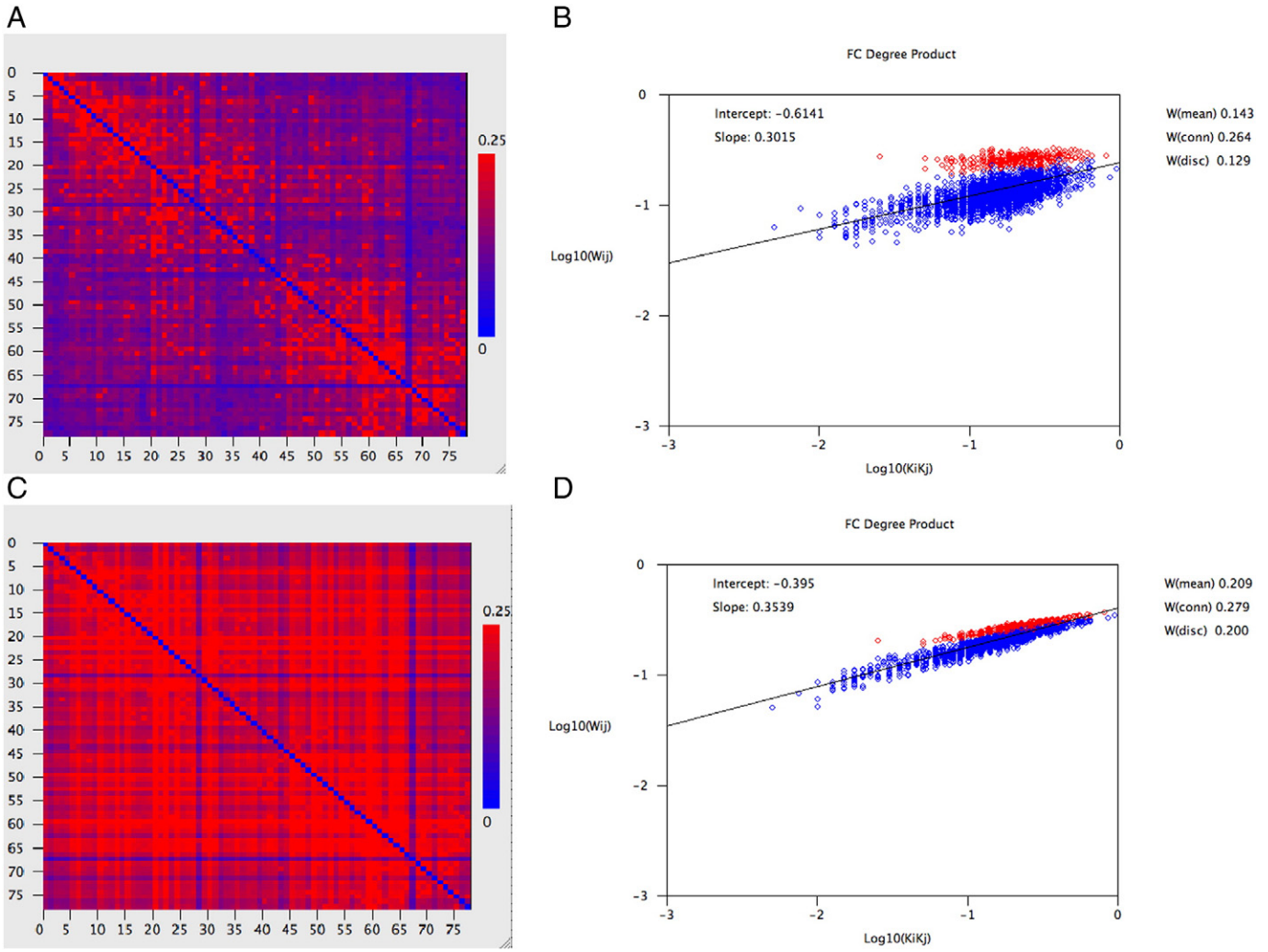

Fig. 9. Functional and effective connectivity for degree preserved random network. Results for degree preserving randomized versions of the original structural matrix. (A) Average functional connectivity matrix based upon 100 runs of 4096 time steps with $\beta = 0.08$ and $\delta = 0.5$. (B) Double logarithmic plot of average functional connectivity as a function of the degree product. The pattern is comparable to the one in Fig. 5B. (C) Average effective connectivity matrix for $\beta = 0.08$ and $\delta = 0.5$. (D) Double logarithmic plot of effective connectivity as a function of degree product. The pattern is similar to the one in Fig. 8B, but with a smaller slope.

that simulate brain dynamics on empirically determined structural networks also suggest that the most meaningful structure function relations are found when the system is near a critical state (Rubinov et al., 2011; Deco et al., 2013). The macroscopic critical state could be related to the existence of so-called neuronal avalanches, bursts of neural activity characterized by power laws, that have been observed in cultured neural networks, local field potentials in monkeys and MEG recordings in humans (Beggs and Plenz, 2003; Yu et al., 2013). Critical dynamics could be the result of a critical branching process or a process of self-organization whereby structural networks constrain dynamical processes, which in their turn may shape the underlying structure (Rubinov et al., 2011; Shew and Plenz, 2013). Critical dynamics may be important from a functional point of view since this critical state has been associated with an optimal sensitivity to input, a maximization of the number of different functional states available (Deco et al., 2013; Shew and Plenz, 2013). Also, it is known from statistical physics that near a critical phase transition the details of the system become relatively unimportant. This might explain why structure function relationships previously observed with very complex realistic models (Honey et al., 2007, 2009) can be replicated with simple dynamic models (Deco et al., 2012; Haimovici et al., 2013).

Table 1
Average results with standard deviation (S.D.) of 20 simulations, each consisting of 100 runs for the original structural network and random networks with preserved degree distribution. Intercept: intercept of linear regression of weight as function of degree product. Slope: slope for the linear regression of the weight against the degree product. W(mean): average weight of both directly and indirectly connected nodes. W(conn): same as W(mean) but only for directly connected nodes. W(disc) same but only for indirectly connected nodes. Significant differences compared to random networks with $p < 0.05$ are indicated in bold.

	Intercept	Slope	W(mean)	W(conn)	W(disc)
Fun conn	−0.627	0.328	0.137	**0.304**	0.116
S.D.	0.044	0.026	0.007	0.011	0.007
Random	−0.646	0.327	0.129	0.251	0.114
S.D.	0.038	0.025	0.008	0.010	0.008
Eff conn	−0.406	**0.448**	**0.174**	0.258	**0.164**
S.D.	0.016	0.007	0.006	0.009	0.006
Random	−0.412	0.378	0.193	0.262	0.184
S.D.	0.015	0.015	0.005	0.005	0.004

We used two different measures to characterize the statistical dependencies between time series of node activation: a functional connectivity measure, based upon the correlation coefficient of integrated node activation time series, and an effective connectivity measure, based upon the probability of time-delayed conditional activation. These measures were intended as simplified versions of the functional and effective connectivity measures used for fMRI BOLD, EEG and MEG studies (Pereda et al., 2005; Friston et al., 2013). Results for the functional connectivity measure resembled those obtained for functional connectivity

analysis of BOLD time series, both in empirical as well as model studies (Honey et al., 2007, 2009; Rubinov et al., 2009; Deco et al., 2012, 2013). Of interest, this result was obtained without using a sophisticated balloon windkessel model (Friston et al., 1995). Again this might be an example of universality near a critical point.

Results for the effective connectivity measure were rather different from those obtained with functional connectivity. The effective connectivity networks did not closely resemble the underlying structural networks, but seemed to be shaped especially by strong connections between high degree hubs, in particular in the posterior part of the default mode network. Of interest, a somewhat similar pattern is observed in source space MEG networks based upon the phase lag index, a measure of time-delayed phase synchronization (Tewarie et al., 2013). In contrast to the functional connectivity, the effective connectivity showed a significant difference in the comparison between the original and the random networks. This suggests that the effective connectivity network may contain information beyond the degree distribution of the underlying structural network. Apparently functional and effective connectivity measures detect different aspects of communication between brain areas, and both are useful to obtain a full understanding of the structure function relations, even in a simple model.

The present study confirmed that functional interactions are stronger between structurally directly connected nodes, in agreement with many previous empirical and model studies (Honey et al., 2007, 2009; Rubinov et al., 2009; Deco et al., 2012, 2013). The great challenge however is to understand what happens when two brain areas do not have a direct connection (Park and Friston, 2013). Functional interactions between indirectly connected brain areas constitute the "dark matter" of brain network studies. We will discuss several possible explanations and relate them to the findings of the present study. The first possibility is that such interactions are caused by volume conduction. This is especially a problem with EEG and MEG, but can be addressed by studying networks in source space and using coupling measures that are insensitive to volume conduction (Hillebrand et al., 2012). Second, it has been suggested that a larger distance between brain areas might determine a lower strength of the functional interactions. A problem here is that the presence and strength of true anatomical connections might also decrease with distance (Markov et al., 2013). A third possibility is that a common driver that influences both areas may determine connectivity. There is evidence that some of the observed functional connectivity could be explained by paths of length two (Honey et al., 2009). In fact the third mechanism is a specific example of a more general mechanism, whereby functional interactions between two areas are determined by indirect connections between them of any length. In a connected graph many such connections of different lengths can be expected to exist, but it is not trivial to understand their influence.

Our results may shed some light on the problem of functional interactions between nodes without direct structural connections. First, volume conduction was not an issue in our model, and all structural connections had unit strength, independent of any distance. Still, we observed a clear relation between structural degree product and connectivity for indirectly connected areas, especially with the effective connectivity measure. *This suggests that the structural degree product of two areas is strongly predictive of the intensity of the traffic between them, even if no direct connection exists. This result shows a striking resemblance to the findings of* Barrat et al. (2004). *In that study the number of passengers traveling between any two airports could be predicted by the degree product of these airports with a scaling exponent of 0.5, close to our observed value of 0.448* (Table 1). The structural degree of a brain area can be understood as an indicator of the probability that this area will "send" activation to the rest of the network as well as the probability that it will "pick up" activity from the network. This may explain why the strength of functional interactions between brain areas, even when they are not directly connected, is related to their degree product. Such interactions between indirectly connected areas will not be picked up by all connectivity measures equally well, and will be obscured by reducing the weighted matrix to a binary graph.

This study has some limitations. First, we used one relatively small structural connectivity matrix as the basis of the model studies. This empirical matrix was based upon DTI tractography that may miss many, especially weak, long distance and crossing connections. Furthermore, recent anatomical work suggests that true brain networks may be less sparse than previously assumed (Markov et al., 2013). Second, while the simplified dynamical model performed quite well in relating structure to function near the critical state, some of the new findings, in particular with respect to the influence of the degree product on functional interactions, need to be confirmed in more realistic models and empirical studies.

5. Conclusion

This study showed that near a critical state a highly simplified dynamical model could provide insight into the relation between structural and functional brain networks. Depending on the connectivity measure used, a close resemblance to the structural network or a clear dependence on the degree product could be demonstrated. This result points the way toward the development of new connectivity measures that may extract the full information available in the functional networks. Also, this type of model might be a fruitful base to study the nature of structure function relations in neurological disorders including epilepsy and neurodegenerative disease.

Acknowledgments

The authors would like to thank Prof Christian Beaulieu, Scientific Director of Peter S Allen MRI Research Centre, Biomedical Engineering, University of Alberta for permission to use the human DTI matrix data.

References

Barabasi, A.L., Albert, R., 1999. Emergence of scaling in random networks. Science 286 (5439), 509–512 (Oct 15).
Barrat, A., Barthélemy, M., Pastor-Satorras, R., Vespignani, A., 2004. The architecture of complex weighted networks. Proc. Natl. Acad. Sci. U. S. A. 101 (11), 3747–3752 (Mar 16).
Bassett, D.S., Bullmore, E., 2006. Small-world brain networks. Neuroscientist 12 (6), 512–523 (Dec).
Beggs, J.M., Plenz, D., 2003. Neuronal avalanches in neocortical circuits. J Neurosci. 23 (35), 11167–11177.
Boguñá, M., Castellano, C., Pastor-Satorras, R., 2013. Nature of the epidemic threshold for the susceptible–infected–susceptible dynamics in networks. Phys. Rev. Lett. 111 (6), 068701 (Aug 9).
Bullmore, E., Sporns, O., 2009. Complex brain networks: graph theoretical analysis of structural and functional systems. Nat. Rev. Neurosci. 10 (3), 186–198 (Mar).
Castellano, C., Pastor-Satorras, R., 2010. Thresholds for epidemic spreading in networks. Phys. Rev. Lett. 105 (21), 218701 (Nov 19).
de Haan, W., Mott, K., van Straaten, E.C., Scheltens, P., Stam, C.J., 2012. Activity dependent degeneration explains hub vulnerability in Alzheimer's disease. PLoS Comput. Biol. 8 (8), e1002582.
Deco, G., Jirsa, V.K., McIntosh, A.R., 2011. Emerging concepts for the dynamical organization of resting-state activity in the brain. Nat. Rev. Neurosci. 12 (1), 43–56 (Jan).
Deco, G., Senden, M., Jirsa, V., 2012. How anatomy shapes dynamics: a semi-analytical study of the brain at rest by a simple spin model. Front. Comput. Neurosci. 6, 68 (Sep 20).
Deco, G., Ponce-Alvarez, A., Mantini, D., Romani, G.L., Hagmann, P., Corbetta, M., 2013. Resting-state functional connectivity emerges from structurally and dynamically shaped slow linear fluctuations. J. Neurosci. 33 (27), 11239–11252 (Jul 3).
Friston, K.J., Frith, C.D., Turner, R., Frackowiak, R.S., 1995. Characterizing evoked hemodynamics with fMRI. Neuroimage 2 (2), 157–165 (Jun).
Friston, K., Moran, R., Seth, A.K., 2013. Analysing connectivity with Granger causality and dynamic causal modelling. Curr. Opin. Neurobiol. 23 (2), 172–178 (Apr).
Gong, G., He, Y., Concha, L., Lebel, C., Gross, D.W., Evans, A.C., Beaulieu, C., 2009. Mapping anatomical connectivity patterns of human cerebral cortex using in vivo diffusion tensor imaging tractography. Cereb. Cortex 19 (3), 524–536.
Gerstein, G.L., Aertsen, A.M., 1985. Representation of cooperative firing activity among simultaneously recorded neurons. J. Neurophysiol. 54 (6), 1513–1528 (Dec).
Guimerà, R., Nunes Amaral, L.A., 2005. Functional cartography of complex metabolic networks. Nature 433 (7028), 895–900 (Feb 24).
Haimovici, A., Tagliazucchi, E., Balenzuela, P., Chialvo, D.R., 2013. Brain organization into resting state networks emerges at criticality on a model of the human connectome. Phys. Rev. Lett. 110 (17), 178101 (Apr 26).

Hermundstad, A.M., Bassett, D.S., Brown, K.S., Aminoff, E.M., Clewett, D., Freeman, S., Frithsen, A., Johnson, A., Tipper, C.M., Miller, M.B., Grafton, S.T., Carlson, J.M., 2013. Structural foundations of resting-state and task-based functional connectivity in the human brain. Proc. Natl. Acad. Sci. U. S. A. 110 (15), 6169–6174 (Apr 9).

Hillebrand, A., Barnes, G.R., Bosboom, J.L., Berendse, H.W., Stam, C.J., 2012. Frequency-dependent functional connectivity within resting-state networks: an atlas-based MEG beamformer solution. Neuroimage 59 (4), 3909–3921 (Feb 15).

Honey, C.J., Sporns, O., 2008. Dynamical consequences of lesions in cortical networks. Hum. Brain Mapp. 29 (7), 802–809 (Jul).

Honey, C.J., Kötter, R., Breakspear, M., Sporns, O., 2007. Network structure of cerebral cortex shapes functional connectivity on multiple time scales. Proc. Natl. Acad. Sci. U. S. A. 104 (24), 10240–10245 (Jun 12).

Honey, C.J., Sporns, O., Cammoun, L., Gigandet, X., Thiran, J.P., Meuli, R., Hagmann, P., 2009. Predicting human resting-state functional connectivity from structural connectivity. Proc. Natl. Acad. Sci. U. S. A. 106 (6), 2035–2040 (Feb 10).

Honey, C.J., Thivierge, J.P., Sporns, O., 2010. Can structure predict function in the human brain? Neuroimage 52 (3), 766–776 (Sep).

Kaiser, M., 2013. The potential of the human connectome as a biomarker of brain disease. Front. Hum. Neurosci. 7, 484 (Aug 15).

Kaiser, M., Hilgetag, C.C., 2010. Optimal hierarchical modular topologies for producing limited sustained activation of neural networks. Front. Neuroinform. 4, 8 (May 14).

Markov, N.T., Ercsey-Ravasz, M., Van Essen, D.C., Knoblauch, K., Toroczkai, Z., Kennedy, H., 2013. Cortical high-density counterstream architectures. Science 342 (6158), 1238406.

Maslov, S., Sneppen, K., 2004. Detection of topological patterns in protein networks. Genet. Eng. (N.Y.) 26, 33–47.

Newman, M.E.J., Girvan, M., 2004. Finding and evaluating community structure in networks. Phys. Rev. E 69, 06113.

O'Dea, R., Crofts, J.J., Kaiser, M., 2013. Spreading dynamics on spatially constrained complex brain networks. J. R. Soc. Interface 10 (81), 20130016 (Feb 13).

Park, H.J., Friston, K., 2013. Structural and functional brain networks: from connections to cognition. Science 342 (6158), 1238411 (Nov 1).

Pereda, E., Quiroga, R.Q., Bhattacharya, J., 2005. Nonlinear multivariate analysis of neurophysiological signals. Prog. Neurobiol. 77 (1–2), 1–37 (Sep–Oct).

Ponten, S.C., Daffertshofer, A., Hillebrand, A., Stam, C.J., 2010. The relationship between structural and functional connectivity: graph theoretical analysis of an EEG neural mass model. Neuroimage 52 (3), 985–994 (Sep).

Rubinov, M., Sporns, O., van Leeuwen, C., Breakspear, M., 2009. Symbiotic relationship between brain structure and dynamics. BMC Neurosci. 10, 55 (Jun 2).

Rubinov, M., Sporns, O., Thivierge, J.P., Breakspear, M., 2011. Neurobiologically realistic determinants of self-organized criticality in networks of spiking neurons. PLoS Comput. Biol. 7 (6), e1002038 (Jun).

Shew, W.L., Plenz, D., 2013. The functional benefits of criticality in the cortex. Neuroscientist 19 (1), 88–100 (Feb).

Sporns, O., 2013. Network attributes for segregation and integration in the human brain. Curr. Opin. Neurobiol. 23 (2), 162–171 (Apr).

Stam, C.J., van Straaten, E.C., 2012. The organization of physiological brain networks. Clin. Neurophysiol. 123 (6), 1067–1087 (Jun).

Stam, C.J., Hillebrand, A., Wang, H., Van Mieghem, P., 2010. Emergence of modular structure in a large-scale brain network with interactions between dynamics and connectivity. Front. Comput. Neurosci. 4.

Tewarie, P., Hillebrand, A., Schoonheim, M.M., van Dijk, B.W., Geurts, J.J., Barkhof, F., Polman, C.H., Stam, C.J., 2013. Functional brain network analysis using minimum spanning trees in Multiple Sclerosis: an MEG source-space study. Neuroimage http://dx.doi.org/10.1016/j.neuroimage.2013.10.022 (Oct 22, pii: S1053-8119(13)01045-8, [Epub ahead of print]).

Tewarie, P., Hillebrand, A., van Dellen, E., Schoonheim, M.M., Barkhof, F., Polman, C.H., Beaulieu, C., Gong, G., van Dijk, B.W., Stam, C.J., 2014. Structural degree predicts functional network connectivity: a multimodal resting-state fMRI and MEG study. Neuroimage 97, 296–307.

Tzourio-Mazoyer, N., Landeau, B., Papathanassiou, D., Crivello, F., Etard, O., Delcroix, N., Mazoyer, B., Joliot, M., 2002. Automated anatomical labeling of activations in SPM using a macroscopic anatomical parcellation of the MNI MRI single-subject brain. Neuroimage 15 (1), 273–289 (Jan).

van Dellen, E., Hillebrand, A., Douw, L., Heimans, J.J., Reijneveld, J.C., Stam, C.J., 2013. Local polymorphic delta activity in cortical lesions causes global decreases in functional connectivity. Neuroimage 83C, 524–532 (Jun 12).

van den Heuvel, M.P., Hulshoff Pol, H.E., 2010. Exploring the brain network: a review on resting-state fMRI functional connectivity. Eur. Neuropsychopharmacol. 20 (8), 519–534 (Aug).

van den Heuvel, M.P., Sporns, O., 2013. Network hubs in the human brain. Trends Cogn. Sci. http://dx.doi.org/10.1016/j.tics.2013.09.012 (Oct 26, pii: S1364-6613(13)00216-7, [Epub ahead of print]).

van den Heuvel, M.P., Stam, C.J., Boersma, M., Hulshoff Pol, H.E., 2008. Small-world and scale-free organization of voxel-based resting-state functional connectivity in the human brain. Neuroimage 43 (3), 528–539 (Nov 15).

van den Heuvel, M.P., Stam, C.J., Kahn, R.S., Hulshoff Pol, H.E., 2009. Efficiency of functional brain networks and intellectual performance. J. Neurosci. 29 (23), 7619–7624 (Jun 10).

van den Heuvel, M.P., Kahn, R.S., Goñi, J., Sporns, O., 2012. High-cost, high-capacity backbone for global brain communication. Proc. Natl. Acad. Sci. U. S. A. 109 (28), 11372–11377 (Jul 10).

Van Mieghem, P., 2012. Epidemic phase transition of the SIS-type in networks. Europhys. Lett. (EPL) 97, 48004 (Februari).

Van Mieghem, P., 2013. Double orthogonality and the nature of networks. Delft University of Technology (report20130923, http://www.nas.ewi.tudelft.nl/people/Piet/papers/TUD20130923_Double_orthogonality.pdf).

Van Mieghem, P., van de Bovenkamp, R., 2013. Non-Markovian infection spread dramatically alters the SIS epidemic threshold in networks. Phys. Rev. Lett. 110 (10), 108701 (March).

Van Mieghem, P., Omic, J.S., Kooij, R.E., 2009. Virus spread in networks. IEEE/ACM Trans. Netw. 17 (1), 1–14 (February).

van Straaten, E.C., Stam, C.J., 2013. Structure out of chaos: functional brain network analysis with EEG, MEG, and functional MRI. Eur. Neuropsychopharmacol. 23 (1), 7–18 (Jan).

Wang, H., Li, Q., D'Agostino, G., Havlin, S., Stanley, H.E., Van Mieghem, P., 2013. Effect of the interconnected network structure on the epidemic threshold. Phys. Rev. E Stat. Nonlin. Soft Matter Phys. 88 (2), 022801 (Aug).

Watts, D.J., Strogatz, S.H., 1998. Collective dynamics of 'small-world' networks. Nature 393 (6684), 440–442 (Jun 4).

Yu, S., Yang, H., Shriki, O., Plenz, D., 2013. Universal organization of resting brain activity at the thermodynamic critical point. Front. Syst. Neurosci. 7, 42 (Aug 22).